Univerzita Karlova
Přírodovědecká fakulta
Ústav hydrogeologie, inženýrské geologie a užité geofyziky

Studijní program: Geologie
Studijní obor: Geologie

Francesco Colosimo

Výpočet magnituda v reálném čase ze záznamů nízkonákladových MEMS akcelerometrů

Real-time magnitude estimation using MEMS-based accelerometers

BAKALÁŘSKÁ PRÁCE

Vedoucí závěrečné práce: Dr. Václav Kuna

Praha, 2022

Prohlašuji, že jsem závěrečnou práci zpracoval samostatně a že jsem uvedl všechny použité informační zdroje a literaturu. Tato práce ani její podstatná část nebyla předložena k získání jiného nebo stejného akademického titulu.

V Praze, 7.5.2022

Francesco Colosimo

Abstract

Earthquakes can be catastrophic events and disrupt people's lives in a significant and uncontrollable ways. Earthquake early warning (EEW) can help to reduce earthquake's impact and provide people with a technology that gives them time for action before destructive waves strike.

This thesis contributes to the development of OpenEEW/Grillo system, by improving an algorithm for magnitude estimation. The thesis consists of two parts, the first part explains the concept of EEW and compares different approaches to EEW and various magnitude estimation algorithms. The second part is observational and uses seismic data from Grillo/OpenEEW network in Mexico. We use data from 1559 earthquakes recorded at the network from 2017 to 2021 and analyse the peak ground displacement with respect to the earthquake magnitude. We observe that earthquake magnitude correlates well with the peak ground displacement and the length of the P-wave segment used in the analysis. We estimate linear regression parameters for P-wave segments up to 10 s long and express earthquake magnitude as the function of peak ground displacement and the length of the P-wave segment.

This work improves the magnitude estimation in the Grillo/OpenEEW system and enables the system to calculate the magnitude using the entire P-wave segment available, which results in quicker and gradually more precise magnitude determination.

Abstrakt

Zemětřesení mohou být katastrofální události a narušit životy lidí významným a nekontrolovatelným způsobem. Včasné varovné systémy před zemětřesením (EEW) mohou pomoci snížit dopady zemětřesení a poskytnout čas, nezbytný k rychlé akci před příchodem ničivých vln. Tato práce přispívá k vývoji systému OpenEEW/Grillo vylepšením algoritmu pro odhad magnituda.

Práce se skládá ze dvou částí, první část vysvětluje koncept EEW a jsou v ní porovnány různé přístupy a algoritmy odhadu magnituda. Druhá část je observační a využívá seismická data ze sítě Grillo/OpenEEW v Mexiku. Pomocí dat z 1559 zemětřesení zaznamenaných seismickou sítí v letech 2017 až 2021 analyzujeme maximální posunutí povrchu země při zemětřesení s ohledem na magnitudo zemětřesení. Pozorujeme, že velikost zemětřesení dobře koreluje s maximálním posunutím země a délkou segmentu P-vlny použité v analýze. Odhadujeme parametry lineární regrese pro segmenty P-vlny dlouhé až 10 s a vyjadřujeme velikost zemětřesení jako funkci maximálního posunutí země a délky segmentu P-vlny.

Tato práce zlepšuje odhad velikosti v systému Grillo/OpenEEW a umožňuje systému vypočítat velikosti pomocí celého dostupného segmentu P-vlny, což vede k rychlejšímu a přesnějšímu určení magnituda zemětřesení.

Poděkování

Rád bych poděkoval všem, kdo se podíleli na vzniku mé bakalářské práce. Zejména chci poděkovat vedoucímu práce Dr. Václavu Kunovi, za možnost zabývat se takto zajímavým tématem, podílet se na praktickém projektu a za nesčetné korektury a trpělivost. Taktéž děkuji rodičům a mé přítelkyni za trpělivost a neustálou podporu v mých studiích.

Contents

1. Introduction

Earthquakes are among the natural phenomena that endanger human populations. Earthquake casualties are generally caused by indirect earthquake effects such as collapse of human-made structures, fires, tsunamis, and avalanches (Snieder et al., 1997). Up to 20% of the global population resides in earthquake-prone areas, estimated to cover 1.369 107 km^2 of the global terrestrial area (He et al., 2021). These regions are irregularly distributed globally, concentrated especially in countries along the Circum-Pacific Belt and the Mediterranean-Asiatic Belt (He et al., 2021).

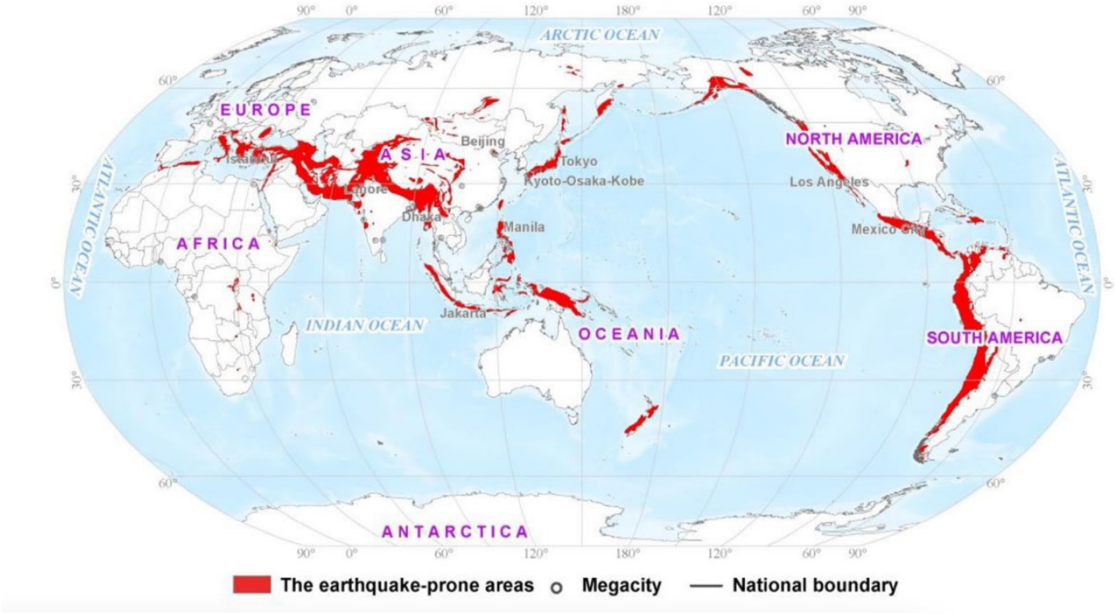

Figure 1. World map with highlighted earthquake prone areas, that stretch along the Circum - Pacific Belt and the Mediterranean-Asiatic Belt (He et al., 2021)

Earthquake-prone areas are located in intraplate regions and along tectonic boundaries, where stress builds up due to movement of tectonic plates. When stress overcomes friction between the two blocks, energy is released and it travels as earthquake waves through the earth. Mitigating the seismic hazard in seismically active regions has been the goal of many researchers and engineers worldwide. Earthquake prediction meant as making deterministic predictions about the location, time, and magnitude of the event may very well be impossible (Snieder et al., 1997). However, with the invention of electronic communication systems, faster than seismic waves, such as telegraphs in the 19th century, they've developed the concept called earthquake early warning (EEW). The alert, thanks to fast communication systems, can

potentially reach the endangered area before the destructive waves arrive. This concept has seen the most significant improvements with the advent of modern information technologies, such as Internet.

This study is composed of two parts, structured around the central theme of earthquake early warning algorithms. The first part is a review about EEW systems, analysing the different approaches and their development, with an insight look into the "Grillo" network.

The second part is an observation of the data taken from the "Grillo" network, that we analysed looking to find new ways optimize the magnitude estimation algorithm.

2. What is Earthquake Early Warning?

Earthquake early-warning systems attempt to detect and characterize earthquakes shortly after their origin. When the system detects an event that is likely to cause shaking that exceeds a certain ground motion threshold, pre-set based on the system's aim and user's needs, it alerts the area where the shaking can potentially hit.

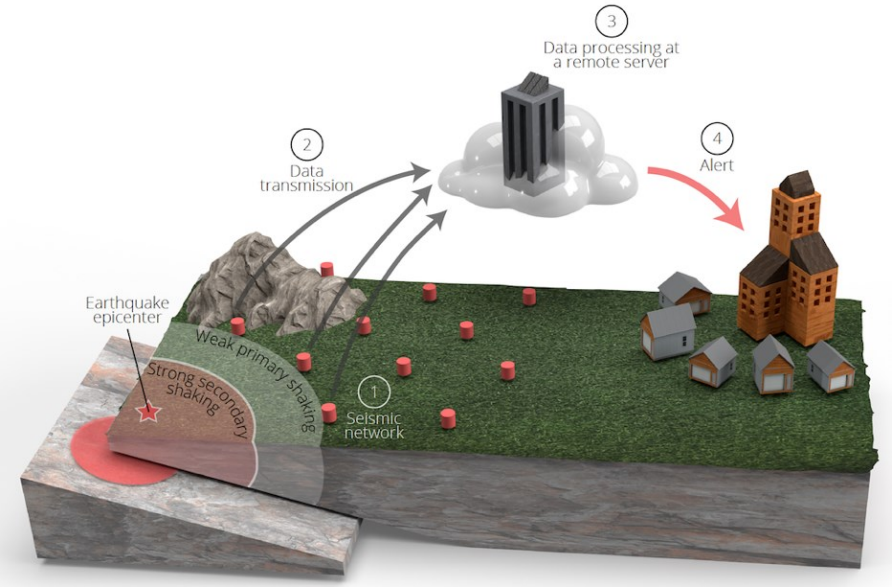

Figure 2. A brief description of a regional EEW system. Highlighting the different steps that lead to the alert. (1) Earthquake waves are detected by a seismic network. (2) The data acquired is transferred to a physical or cloud server where the data is processed (3), and magnitude is calculated. (4) If the parameters calculated by the analysis require so, an alert is released (Kuna pers. comm.)

There are many variants and adaptations of this system because of a big variability of users and the geological context in which the system operates. Each variant might work with different earthquake parameters, but fundamental physics laws are often the biggest limits of these systems.

Earthquake early-warning systems today are being developed and tested in multiple countries, delivering public alerts in Mexico, Japan, South Korea, and Taiwan and alerts to select user groups in India, Turkey, Romania, and the United States (Allen and Melgar, 2019).

The system can have different components, physical and software, and follows different steps in the magnitude estimation and alert. The ground motion is picked-up by the seismic network that transmits data either to the cloud or to physical servers, where the data processing and the actual estimation and data analysis happens. After having evaluated the magnitude an alert is released if needed.

2.1. Approaches to EEW

EEW systems have different approaches to alert generation. Three main algorithms have been developed, each with a slightly different aim. (Allen and Melgar, 2019)

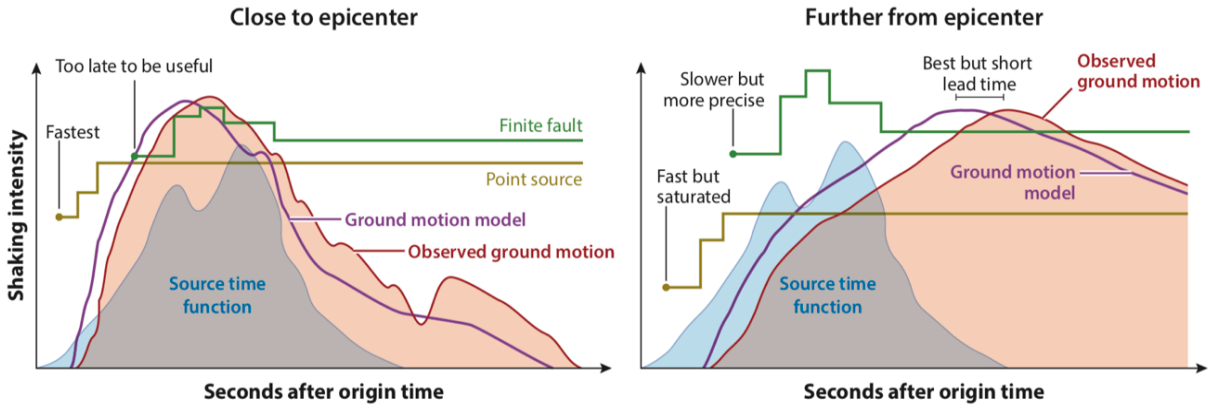

Fugure 3. Comparison how the different algorithms behave in two different scenarios: close and farther from the epicentre. The point source is the fastest, in both scenarios, but doesn't reach the precision of the finite fault algorithm. We see that the point source algorithm struggles to measure the strongest intensities as it saturates for strong magnitudes. (Allen and Melgar, 2019)

- Point source algorithms provide the fastest estimation of earthquake parameters (i.e., giving the most warning time), using just a few seconds of P-wave data (0.5–10 s) from a few stations closest to the epicentre. They detect an earthquake and determine its location and magnitude, which can be translated into ground shaking prediction by employing an appropriate ground motion prediction equation (GMPE). However, magnitude estimation saturates for more significant earthquakes (usually ~M6.5; Li et al., 2017) as seismic waves of such large earthquakes are almost impossible to differentiate when only a few seconds of the record are available (Allen and Melgar. 2019).

- Finite fault algorithms aim to overcome the point source saturation issue by estimating the finite extent of the rupture using seismic and geodetic approaches. Although these algorithms are slower than point source, they can estimate strong earthquake intensities with higher accuracy (Allen and Melgar. 2019).

- Ground-motion models (GMMs) are very different, using observations of strong shaking to alert of imminent tremors at other locations without analysing the source. Therefore, they do not have to address earthquake analysis problems. The disadvantage is that the accuracy of the ground shaking prediction decreases as a function of the warning time (Allen and Melgar. 2019).

2.2. Point source algorithms

Point source algorithms are used in two different earthquake early warning approaches based on the geographical layout of the sensors (Allen and Melgar, 2019).

Single-station EEWs use the first few seconds of P-wave to predict the peak ground acceleration (PGA), related to slower S–waves, at that same site and are suitable for locations closer to the earthquake epicentre (Kuna et al., in prep.).

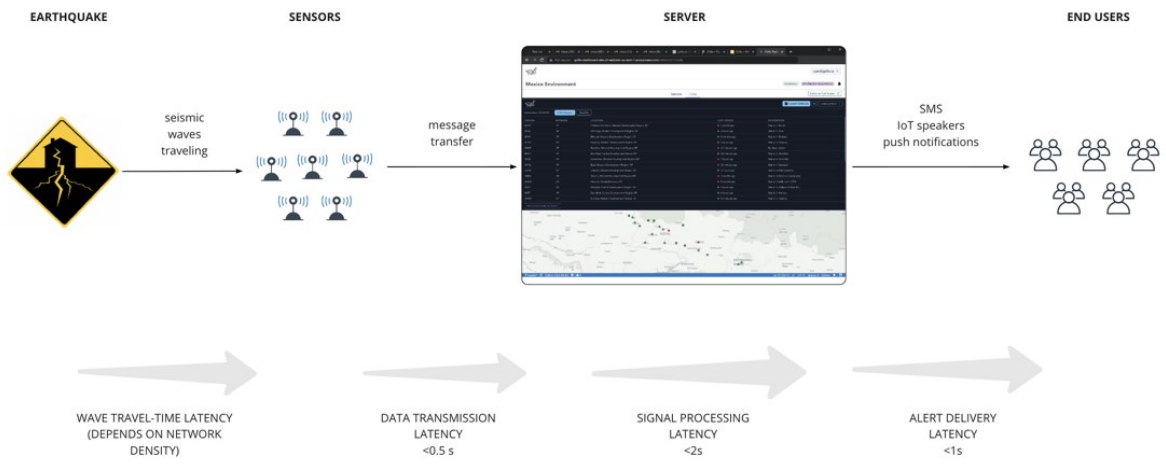

Figure 4. A brief description of a regional EEW systems latency. Highlighting the different times needed for each step of detection, data processing and alert. (Kuna pers. comm.)

Regional EEWs use seismic networks deployed based on the geological knowledge of an area, in or near a determined fault system and aim to detect and characterise earthquakes a few seconds after their origin. Such systems utilise electromagnetic communication that are significantly faster than seismic waves. As a result, regional EEWs can provide useful alerts to sites farther than 50 km from the earthquake epicentre (Kuna et al., in prep.). This is because even when just a few seconds of P-wave is used, it takes some time for the system to process the data and issue an alert, it's called the latency of the system, and it comes mostly from transmission of data, signal processing and alert delivery.

Therefore, the system's latency can be improved by having a denser network of sensors in the region, having a higher probability of being close to the epicentre. Density of the network depends on the budget, a low-cost sensor would then allow for the deployment of large numbers and provide dense station coverage across a large area, improving warning time.

3. Sensors

Besides the algorithm of detection and alert, selecting a suitable sensor is a significant step for the proper operation of the system. There's an extensive range of sensors able to detect ground motion because of considerable variability in the motion itself and the aim of the sensor. Seismometers can be split into two main categories.

Weak motion seismometers, as broadband sensors, are most suitable for measuring small ground motions caused by low magnitude local earthquakes or very distant ones.

Broadbands can record a very broad range of frequencies, having very low self-noise and higher sensitivity. However, because these sensors are optimised for weak-motion signals, they do not cope well with large ground motions induced by stronger earthquakes that will cause "clipping "of the signal or go off-scale (Alaska Earthquake center 2019).

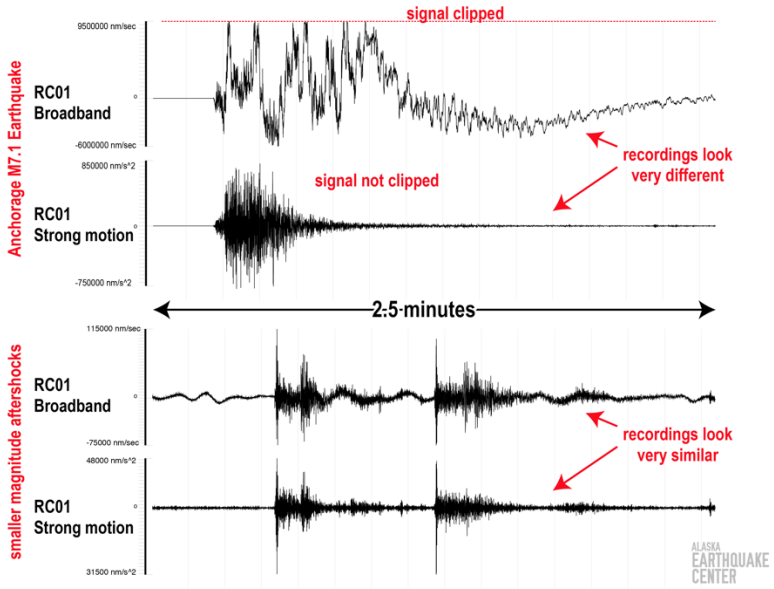

Figure 5. Image taken from the webpage of the Alaska earthquake center. It compares the performance of broadband and strong motion sensors. Recording a strong ground motion, like the one caused by the Mw7.1 Anchorage earthquake, makes the signal from the broadband sensor clip, instead the strong motion sensor is able to record the signal correctly. However, in case of weak motion, as shown in the lower two seismograms, both sensors accurately record the weak motion, caused by smaller aftershock. (University of Alaska Fairbanks, Alaska earthquake center 2019)

Strong-motion seismometers measure acceleration, they are not as sensitive to ground motions as broadband sensors, but they manage to keep the signal on scale during the strongest seismic shaking. The definition of "strong – motion" is a ground motion of sufficient amplitude and duration to potentially damage a building or other structure.

For broader seismological purposes, broadband seismometers are useful, but for the specific needs of EEW systems, strong motion sensors have the best characteristics (Fu et al. 2019).

3.1. MEMS

Micro Electro Mechanical Systems (MEMS) accelerometers are a chip-based technology. These sensors have the potential to replace analogue geophones, becoming a reference for various applications, but the seismic industry hasn't largely adopted them yet (Tellier and Lainé, 2017). Same as geophones, MEMS accelerometers work on the principle of a damped mass-spring system. When the ground shakes, the coil, which works as the proof mass, remains still. At the same time, in geophones, the casing and the magnet move relatively to it, producing an output proportional to the relative displacement rate (velocity).

Instead in MEMS accelerometers, the inertial mass moves in phase with the casing when subjected to seismic waves. Consequently, no relative force is applied to the mass with a constant velocity. Instead, when the sensor is exposed to acceleration, a force is applied to the mass, and digital sensors act as accelerometers and deliver digits proportionally to ground acceleration (Tellier and Lainé, 2017).

MEMS can have different outputs based on how the inertial mass is controlled:

- "Open-loop" MEMS accelerometers have no movement control of the inertial mass. A capacitive position sensor measures changes in position. The acceleration is calculated from the displacement and the spring stiffness and mass.

- "Closed-loop" MEMS accelerometers have movement control of the inertial mass instead. The ground acceleration is calculated by measuring the needed force to keep the inertial mass at its resting position. This force is applied by a voltage on the electrodes that is digitalized as output.

MEMS have relatively high self-noise. It is an output of the sensor without any external perturbations, called Brownian noise, produced by the collision of molecules in the sensing cell. Recent advancements in MEMS technologies have improved the component's quality, reducing self-noise and providing a higher resolution than the older versions.

Therefore, modern MEMS accelerometers are well fitted for early earthquake warning purposes, with low-cost components and lower self-noise than their predecessors.

4. Magnitude calculation

Estimating magnitude is vital for the functioning of an early earthquake warning system, since it has to estimate the size and damage potential for an occurring earthquake.

Different earthquake parameters have been used to estimate magnitude. Searching for the most precise method that requires less time as possible, as for EEW purposes is key to quickly estimate and alert.

4.1 Peak ground acceleration

Peak ground acceleration (PGA) is the amplitude of the largest absolute acceleration that occurred during an earthquake shaking at a location (Douglas, 2003).

There's a relationship between the area covered by the high acceleration levels and their corresponding earthquake magnitudes for large shallow earthquakes (Ting-Li and Yih-Min 2010). During these earthquakes, the logarithm of the area covered by the high levels of PGA contours have a linear correlation with earthquake magnitude. This relationship can estimate magnitude once the strong ground motion covered area is determined (Ting-Li and Yih-Min 2010).

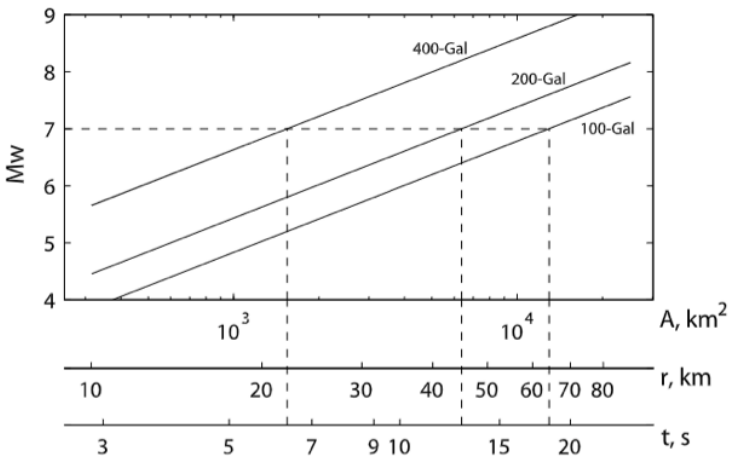

Figure 6. Shows the relationship between the area inside the PGA contour and its actual magnitude. Three values of PGA, of 100, 200,and 400 Gal are used for the contour. The areas (A) are converted to circles to obtain the radiuses (r) and travel time (t) (Ting-Li and Yih-Min 2010)

The accuracy of the calculated area inside a PGA contour depends on the distances between the stations. A dense system of seismic sensors with distances between stations, less than tens of kilometers, can significantly improve the magnitude estimation accuracy *(Ting-Li and Yih-Min 2010)*.

4.2. Peak ground displacement

Peak ground displacement (PGD) is the maximum displacement recorded at a station during an earthquake. PGD has two parts: the transient displacement, which relates to the elastic properties of the earth's crust and at the end of the record should be equal to zero and the displacement due to a permanent movement of the recording station, related to the plastic character of a fault rupture. In 2005, Wu and Kanamori (2005) found that the peak initial displacement amplitude correlates well with the peak ground velocity (PGV) and magnitude. Wu and Li (2006) put forward the empirical relationship between peak displacement and the hypocentral distance R and the magnitude M:

$$\log_{10}\mathrm{Pd} = \mathrm{A} + \mathrm{BM} + \mathrm{C}\log_{10}(\mathrm{R})$$

Pd is the initial displacement after applying a 0.075-Hz high-pass filter, M the magnitude, R the epicentral distance and A, B, and C regression parameters.

Zollo et al. (2006) normalized the Pd parameter to a distance of 10 km and expressed it as:

$$\log\left(PGD_t^{10\ km}\right) = A + BM$$

PGD is the peak ground displacement amplitude after applying a 0.075-Hz high-pass recursive Butterworth filter to remove the low-frequency drift after the numerical integration. M is the magnitude; R is the hypocentral distance and A and B are constants determined by the regression analysis.

4.3. Maximum predominant period, velocity parameters

Nakamura, in 1988, elaborated an algorithm to calculate the predominant seismic period based on real-time velocity records. Allen and Kanamori (2003) believed that the maximum of $\tau_p(I)$, calculated based on the few seconds following the arrival of the P wave, is proportional to the magnitude and so developed an algorithm called τ_p^{max} method. It should be noted that the correlation between τ_p^{max} and the strong magnitude events is not related just to the source characteristics, but it is derived from a combination of attenuation and filtering effects (Wolfe 2006).

$$\log(\tau_p^{max}) = A + BM$$

4.4. Characteristic Period, τc

Kanamori (2005) improved the τ_p^{max} method and proposed the τ_c parameter by integrating with a fixed interval instead of step-by-step. The value of τ_c is the average of the periods within t seconds after the arrival of P waves. τ_c has similar physical meanings with τ_p^{max}. Still, they have different results for the same seismic records, related to the noise level before the P-phase arrival (Shieh et al., 2008).

$$\log(\tau_c) = A + BM$$

4.5. Comparison

Li et al. (2017) compared three methods of magnitude estimation for earthquake early warning purposes. The maximum predominant period τ_p^{max} parameter correlates well with magnitudes in the 4–6 and 6-8 ranges, but with a large standard error and smaller linear slope, especially for the large magnitudes. Instead, the characteristic period τ_c parameter scales with the entire magnitude range without evident saturation. Nevertheless, the linear slope is slightly lower, less predictive for larger magnitudes. Finally, the peak ground displacement parameter is a good estimator of the 4–6 magnitude range, saturating at higher magnitudes. Increasing the

time window length and adjusting the filtering bandwidth can improve the saturation (Li et al., 2017).

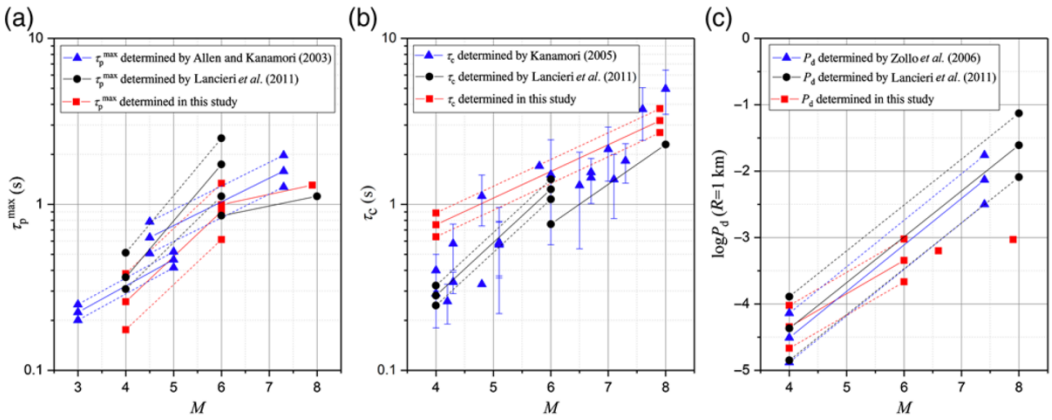

Figure 7. Comparison of three earthquake parameters for magnitude calculation purposes, between different studies. (a) τ_p^{max} models presented by Allen and Kanamori (2003), Lancieri et al. (2011) and Li et al., (2017). (b) τ_c models determined by Kanamori (2005), Lancieri et al. (2011), and Li et al., (2017). (c) Pd models determined by Zollo et al. (2006), Lancieri et al. (2011), and Li et al., (2017). (Li et al., 2017)

5. Alert generation

EEW systems are heavily influenced by users' needs. These systems have to consider that the end output, the alert, has to be easily understood by the general public and not by just a few specialised people, as happens with scientific measurements, for example. Therefore, it is important to have a rapid magnitude determination closely related to the earthquake's damage potential *(Ting-Li and Yih-Min 2010)*. The magnitude estimation or alert generation method must be directed toward the level of strong shaking that is the most important factor in predicting damage potential instead of concerning earthquake energy release. That is why the Modified Mercalli intensity scale is used for an alert generation. Usually, the MMI V is applied as the threshold when EEW is most useful (Allen, Melgar. 2019).

MI V is defined as "felt by nearly everyone; many awakened: Some dishes and windows are broken. Unstable objects are overturned. Pendulum clocks may stop." ("Magnitude vs Intensity". USGS).

Magnitude	Approximate fault length	Approximate distance from fault where MMI ≥ V	Maximum epicentral distance where MMI V is expected	S-wave arrival time at maximum distance where MMI V is expected	Approximate end of peak shaking
M5	1 km	8 km	10 km	4 s	10 s
M6	6 km	30 km	40 km	10 s	20 s
M7	50 km	100 km	200 km	40 s	60 s
M8 (crustal)	400 km	300 km	700 km	200 s	300 s
M9 (subduction)	1,000 km	400 km	1,000 km	300 s	600 s

Table 1. Approximate estimates of distances and times for earthquake early warning purposes (Allen and Melgar. 2019)

This table shows the relation between magnitude, distances and times for EEW purposes. The numbers are only approximate, as the shaking intensity at any specific location can vary by a factor of two (Worden et al. 2010) to the output of the ground motion prediction equations (GMPEs). The strongest shaking doesn't have to be strictly connected to the arrival of the S-wave, as it can occur significantly later. Peak shaking observations for magnitude events larger than 6 show that the strongest shaking can occur up to 10 s after the S-wave at a 50 km distance and up to 50 s at 400 km (Allen 2011). This is a further positive point that increases warning time *(Allen and Melgar. 2019)*.

Having defined the intensity of the shaking at which an alert should be sent out is key, but it's also very important defining the area where the alert should be sent. The area that might be affected by Mw events larger than six can be very large, but most of the damage will almost always be at smaller epicentral distances and close to the rupturing fault. Therefore, timing and sending an initial alert within a few seconds is probably, besides reliability, the most critical objective for an EEW system *(Allen and Melgar. 2019)*. The so-called "Gray zone", where the warning time is larger than the arrival time of the peak shaking, can be reduced as much as possible using this strategy. Usually, the "Gray zone" extends up to 30 km from the epicentre (Tajima, Hayashida, 2018). After this initial alert, there's time to improve the precision of the magnitude estimation and alert in case it's needed in a larger region. As stated before, these early magnitude predictions saturate for stronger magnitudes because often, the rupture time of the fault can be longer than the analysed time window. Also, point-source algorithms don't consider the lateral extent of the rupture, which can be hundreds of kilometres for stronger earthquakes.

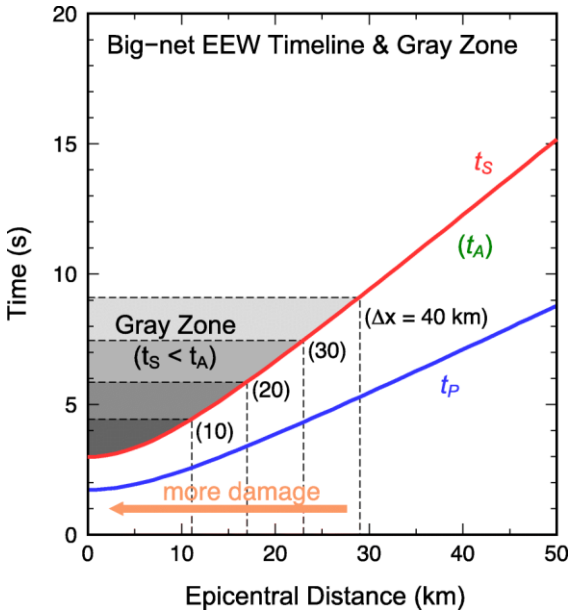

Figure 8. Timeline of EEW alert time (t_A), with gray-zone. The y-axis is the time relative to the origin time of the event, the x-axis epicentral distance. The travel time curves for P- and S-waves (denoted t_P and t_S) are as a function of epicentral distance, assuming 5.8 km/s for P-wave speed and 3.4 km/s for S-wave speed (Tajima and Hayashida. 2018)

Alert generation is the final product of EEW systems; therefore, it has to account for all the complexities of earthquakes and societies. But, on the other hand, having false positives could ruin the system's reputation and society's trust in it, so there has to be a balance between the responsiveness of the system and the reliability of the prediction.

Many things can be implemented in today's EEW systems that could help improve alert generation. For example, today's GMPEs should consider the geology of where the station is located and the user's location, as it has happened many times that a far earthquake damaged densely populated areas because of their location in the geological context.

6. Case study

EEW systems are operational all around the globe, with the most extensive nationwide system being in Japan and operating since 2007. It consists of over 4000 contributing stations, with 15 deep borehole seismometers, added in 2015, to obtain additional lead times and to improve the detection capability for offshore earthquakes *(Tajima and Hayashida. 2018)*. Japan Meteorological Agency (JMA), that operates the system, also incorporated two ocean-bottom

seismometers. Over the last fifteen years, Japan has been hit by some of the strongest earthquakes ever recorded, having a lower number of casualties compared to other countries, because of their building codes and implementation of EEW systems (Tajima and Hayashida, 2018).

Date	Earthquake name	*M*w	Casualties
2001/01/26	Gujarat/India	7.7	13,805~20,023
2003/12/26	Bam/Iran	6.6	31,824~ 43,000
2004/12/26	Indian Ocean/Indonesia	9.1~ 9.3	230,000~280,000
2005/10/08	Kashmir/Pakistan	7.6	Up to ~ 88,000
2008/05/12	Wenchuan/China	7.9	Up to ~ 88,000
2010/01/12	Port-au-Prince/Haiti	7.0	100,000~316,000
2011/03/11	Tohoku-Oki/Japan	9.0–9.1	~ 18,500 (837)

Table 2. List of the deadliest earthquakes of the 21st century (Tajima and Hayashida, 2018)

Deaths caused by an earthquake aren't strictly proportional to magnitudes, as table 1 shows, listing the deadliest events in the last two decades. It highly depends on natural factors such as earthquake depth, time of occurrence (day or night) and local geology, all factors that we cannot influence. But it also depends on government bodies that can implement standard building codes, advanced engineering preparations, monitoring and alert systems such as EEW.

6.1. Mw 9 Tohoku-Oki 2011 case study

The 2011 Mw 9 Tohoku-Oki earthquake was the second strongest of the 21st century but compared to all the other deadliest events of the last two decades it caused the least casualties (Table 2). It caused about 18,500 fatalities and 4% of the total were victims of building collapses or landslides, most of the victims succumbing to tsunamis (Tajima, Hayashida. 2018). In 2011, when this earthquake occurred offshore of Japan, the EEW system detected P-waves ~ 22 s after its origin time and issued the first alert in ~ 8 s from the first P-wave arrival time *(Tajima and Hayashida. 2018)*.

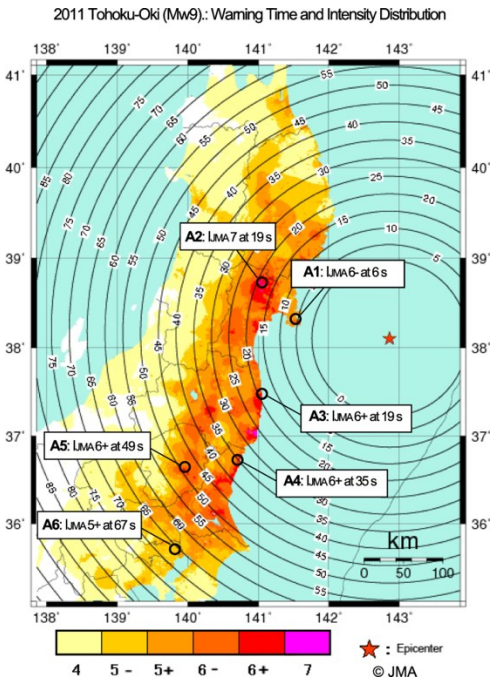

Figure 9. Warning time and intensity for the 2011 Tohoku-Oki earthquake. Here, the warning time is the time between the issue of the alert and S-wave arrivals estimated on concentric circles. (Tajima and Hayashida, 2018)

After the event was detected, an alert was sent to various facilities to take necessary actions. JMA also issued warnings for large tsunamis, but due to the underestimated tsunami heights in the beginning and miscommunication problems, many people were killed (Tajima et al., 2013).

Japan is at the forefront of earthquake early warning technology, with one of the most advanced systems, but it still has quite important shortcomings, which events like the 2011 Tohoku-Oki highlight very well. After the mainshock, the system had some failures due to power outages. This caused false alerts, and the system also failed to detect several significant aftershocks (Hoshiba et al., 2011). Nonetheless, without the EEW system and intensive engineering preparations, casualties and damages would have been fairly higher (Tajima et al., 2013).

The Tohoku earthquake was a benchmark test for the relatively new EEW system. It gave scientists the possibility to analyse the advantages as well as the negatives of such a system.

In the last two decades, approximately 74.5% of the total deaths in global earthquake-prone areas occurred in developing countries (He et al., 2021). This shows how strictly correlated are infrastructures designed to withstand shaking, EEW systems and earthquake casualties. Therefore, it would be necessary to force a big change in the development and urbanisation of such countries, having infrastructures and buildings designed to withstand ground shaking. But,

even in developed countries with seismic building codes, relatively low magnitude earthquakes can cause many casualties.

EEW systems in earthquake-prone areas could make the difference, especially where structural seismic engineering isn't so advanced. Hence, developing a low-cost system that could be adopted by developing countries without the need to invest large amounts of money into sophisticated systems, such as the JMA's EEW, could help save many lives.

6.2. Grillo and OpenEEW

The "Grillo" EEW system has been tested in Mexico since 2017 when 24 seismic sensors were deployed on the southwest coast of the country and three around Mexico City.

The "Grillo" system has been developed with the idea of keeping the cost low while keeping the performance high. Its performance has to be considered in relation to the available budget. The JMA's EEW has a yearly budget of nearly 450 million euros per year (平成 23 年度 気象庁関係予算決定概要. Japan Meteorological Agency. December 24, 2010. Retrieved April 1, 2012.), instead the "Grillo" network using open-source hardware designs is able to dramatically bring the costs down. Of course, expectations for these low–cost systems should be adapted to the budget, but in its short existence, the "Grillo" network deployed in 2017 on the western coast of Mexico already has shown its capabilities during various earthquakes.

The instruments are located in schools, hospitals, and government buildings and are mounted on a primary structural element on the ground level of the building, isolated from surrounding noise. They transmit live, 32 samples-per-second, to the Grillo platform on Amazon Web Services (Kuna et al., in prep.).

6.3. GRILLO/OpenEEW SENSOR

The sensor comprises two major components: the MEMS accelerometer and CPU modules. The MEMS is an ADXL355 triaxial, low-noise, low-power accelerometer, with a full-scale range of ±2g. It has a resolution of ~4 μg/√Hz, and a noise density of 22.5 μg/√Hz in the bandwidth of 0.095-1000 Hz. It includes a 20-bit analogue-to-digital (AD) converter (Kuna et al., in prep.). The CPU modules comprise, in the older versions, a Raspberry Pi 3b, a 1.2 GHz

64 quad-core processor. The latest versions use a low-cost and low-power ESP32 microcontroller with a dual-core Tensilica Xtensa LX6 microprocessor. All hardware components are contained in a custom-designed PCB board with integrated Wi-Fi, Bluetooth, and Ethernet connectivity (Kuna et al., in prep.).

6.4. Grillo Mw 7.1 Guerrero case study 2021

One of the most recent examples of the network's potential has been during the Guerrero event on the 7th of September 2021.

The epicentre was 6 km in front of the coast of Acapulco (*"CATÁLOGO DE SISMOS". Servicio SismológicNacional*). It was a thrust faulting event located in the subduction zone of the Caribbean Plate and Cocos Plate. Its relatively shallow hypocentre, only 20 kilometres below the surface, has probably amplified the shaking effect. The earthquake was located in the southern part of the Guerrero Gap. It is a seismic gap on the subduction boundary which stretches from Acapulco in a North–West direction for 230 km because, in this region, no major earthquakes have struck for over 110 years. *"CATÁLOGO DE SISMOS". Servicio SismológicNacional*). The earthquake affected almost 2 million people in five Mexican states, as reported by local news. It damaged infrastructures also in Mexico City, 300km from the epicentre, as it is located on a sedimentary basin that significantly amplifies the shaking.

During this event, the "Grillo" network worked very well, also because of the location of two stations that were 7 and 11 km from the epicentre. This helped assess the magnitude and deliver the alert in 5 to 6 seconds, with an alert time up to 80 seconds in Mexico City and progressively lower closer to the epicentre.

This event proved the potential of the "Grillo" system, showing the need for a very dense net of stations to significantly improve warning time. Such a low-cost sensor will make this achievable with lower budgets, making earthquake early warning possible even in developing countries.

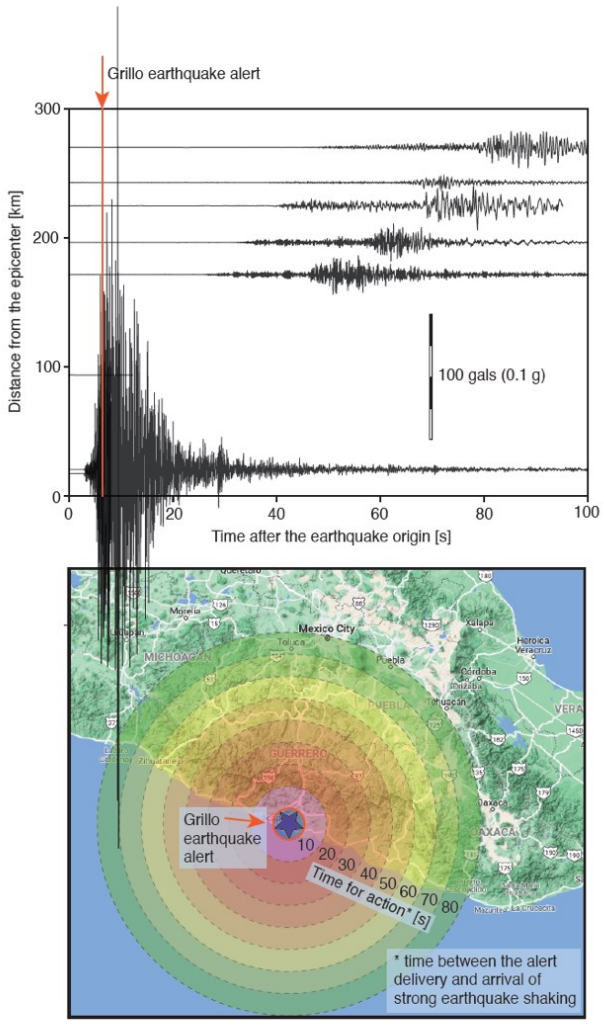

Figure 10. Warning time for the 2021 Guerrero earthquake. Here, the warning time is the time between the issue of the alert and S-wave arrivals estimated on concentric circles. Grillo alert time plotted in the accelerogram of the event. (Kuna pers. comm.)

As of today, the "Grillo – OpenEEW" system is being tested in Mexico and Nepal, with an expansion into Haiti coming soon. The deployment of the system in multiple countries dramatically helps the improvements of the system itself, having more data to analyse and having to cope with very different contexts.

In the next chapter we analyse data from the Mexican network. This allows us to improve the algorithm for magnitude estimation. That, in case of a positive outcome, will then be expanded to all the "Grillo" systems actually deployed.

7. Data

The data analysed, from the Mexican "Grillo" network, is from a three and a half year time span, between November 1, 2017 and September 11, 2021. The dataset is composed of 1605 earthquakes with magnitudes ranging between 4.0 and 7.4, with the June 23, 2020 event being the strongest on record. The sensors recorded 1559 earthquakes of $4 < Mw < 5$; 41 of $5 < Mw < 6$; 2 of $6 < Mw < 7$; and 3 earthquakes of $Mw > 7$ (described in Fig. 11). Earthquake's epicentres follow a NW-SE trend along the Middle America Trench, where the Cocos plate begins its descent into the mantle beneath Mexico, causing this region of the country to be highly seismically active. The sensors have been laid out along the coastline to intercept earlier seismic waves coming from the subduction front to provide earthquake early warnings, with more significant alert time, for the densely populated states farther inland. There happened to be data gaps in data return from the stations, caused primarily by power and connectivity issues, which did not affect in a major way the analysis.

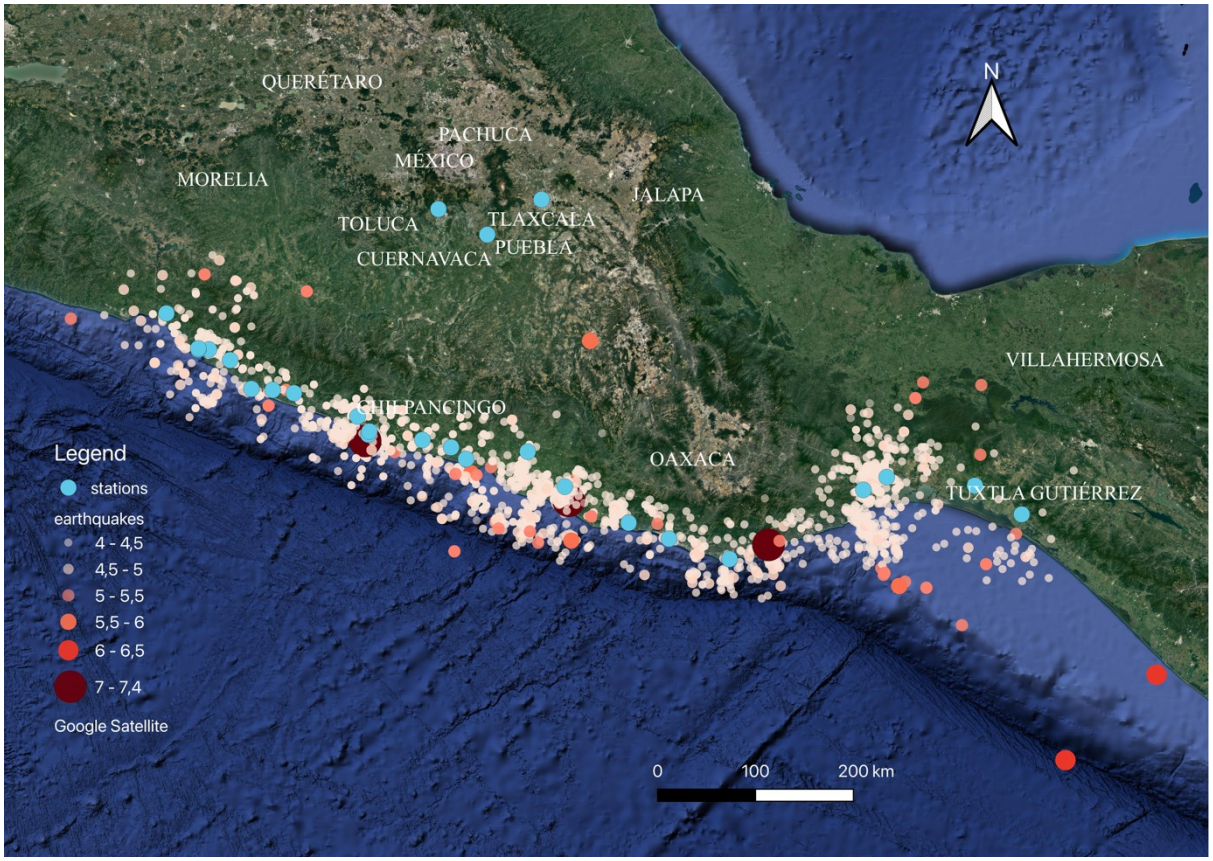

Figure 11. Geographic characterisation of the epicentres in the dataset and the Grillo stations.

Three major earthquakes occurred during the selected time window. The first was the Mw 7.2 “Pinotepa” earthquake (UNAM Seismology Group, 2013, Li et al., 2018), which hit the state of Oaxaca on February 16, 2018. The maximum ground motion reached intensities of VII on the Mercalli scale. The second, 200 km southeast of the “Pinotepa” event, was Mw 7.4 “La Crucecita” earthquake on June 23, 2020, (Melgar et al., 2020; Villafuerte et al., 2020), which caused strong shaking, with a maximum intensity of IX (Kuna et al., in prep.). The third was the Mw 7.1 “Guerrero” earthquake with an estimated intensity of VIII, which caused 13 casualties and affected at least 1.6 million people in Mexico and resulted in localized severe damage. The Grillo sensors recorded these large events across the network.

8. Method

We used the Mexican National Seismological Service (Servicio Sismológico Nacional; 182 SSN) earthquake catalogue to obtain earthquake source parameters (epicentral location, origin time, and magnitude) for events occurring between the studied period. We used the catalogue as an aid for manual picking of P and S phases in our data and performed picking using seismological trace viewer Snuffler (Heimann et al., 2017).

We used Python ObsPy tool for the data processing (Krischer et al., 2015). The traces were demeaned and filtered to remove the low-frequency drift after the integration. We used a 4-pole high pass filter with a 0.075 Hz corner frequency on the acceleration records and a 4-pole bandpass filter 1 to 3 Hz after double integration into displacement. The sensors record ground motion in three orthogonal directions. The PGD was determined as the maximum of the absolute value of the vector sum of the three sensor components.

We corrected the PGD to a common epicentral distance of 10 km.

$$\log\left(PGD_t^{10\ km}\right) = \log(PGD) + 1.38\ log_{10}R \qquad \text{(Kuyuk and Allen 2013)}$$

To correct the early P-wave peak amplitude for the distance attenuation effect, we assumed a simple linear relationship between the logarithmic PGD and the logarithmic epicentral distance (Kuyuk and Allen 2013). To define the correlation between magnitude and PGD we used a

linear regression with the least squares' method. The uncertainties were calculated and plotted as the 95% confidence interval for the estimated regression parameters, using semi-transparent bands around the regression line.

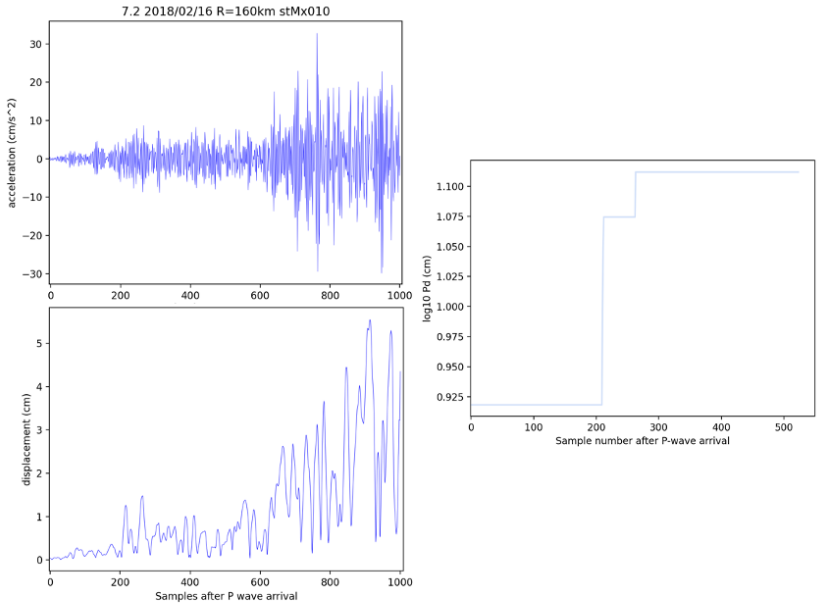

Figure 12. *Three outputs of the Mw 7.2 "Pinotepa" event. Acceleration, the envelope and the* log_{10} *of the displacement. The records are taken from the station Mx010 located 160km from the epicenter. The graphs show the relation between the peaks of acceleration and consequent peaks of displacement. As mentioned in the review section, strong shaking is associated with the arrival of the S-waves, or even later (Allen 2011). This is clearly visible at the S-wave arrival, ~600 samples after the P-wave arrival, where we see a significant raise in acceleration immediately followed by a peak of displacement up to 5 cm.*

We analysed the magnitude estimation with different time windows, looking for signs of saturation in relation to the length of the p-wave data. Because of unbalanced data with most of the earthquakes with 4 to 5 magnitude, we decided to do the regression analysis with the mean of all the measurements for every decimal magnitude.

9. RESULTS

The PGD shows correlation both with the length of the segment P-wave and the earthquake magnitude.

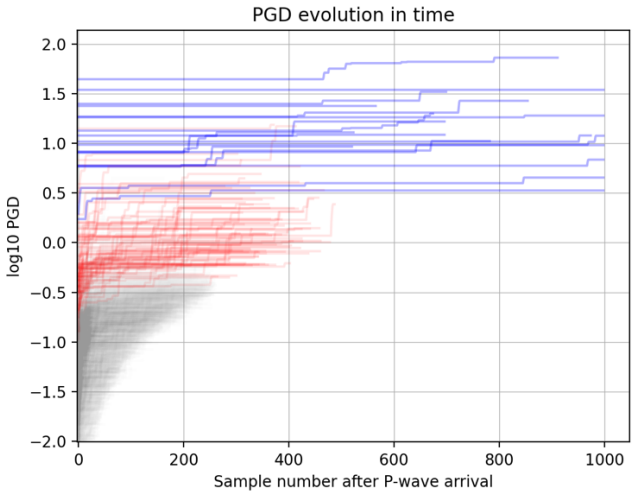

Figure 13. *Time evolution of the log_{10} PGD which demonstrates its correlation with the different time windows. Earthquakes were split into three magnitude categories, 4 to 5, 5 to 6 and larger than 6. The displacement is plotted relative to the number of samples after P – wave arrival (1 second = 32.5 samples).*

We observe significant scaling of the peak ground displacement in the magnitude range between 4 and 7.4 for all time windows, that follows the equation:

$$\log\left(PGD^{10km}\right) = \mathrm{A} + \mathrm{B}\ M$$

where A and B are the parameters calculated from the regression analysis, M the magnitude and PGD ^{10km} the peak ground displacement corrected to a distance of 10km.

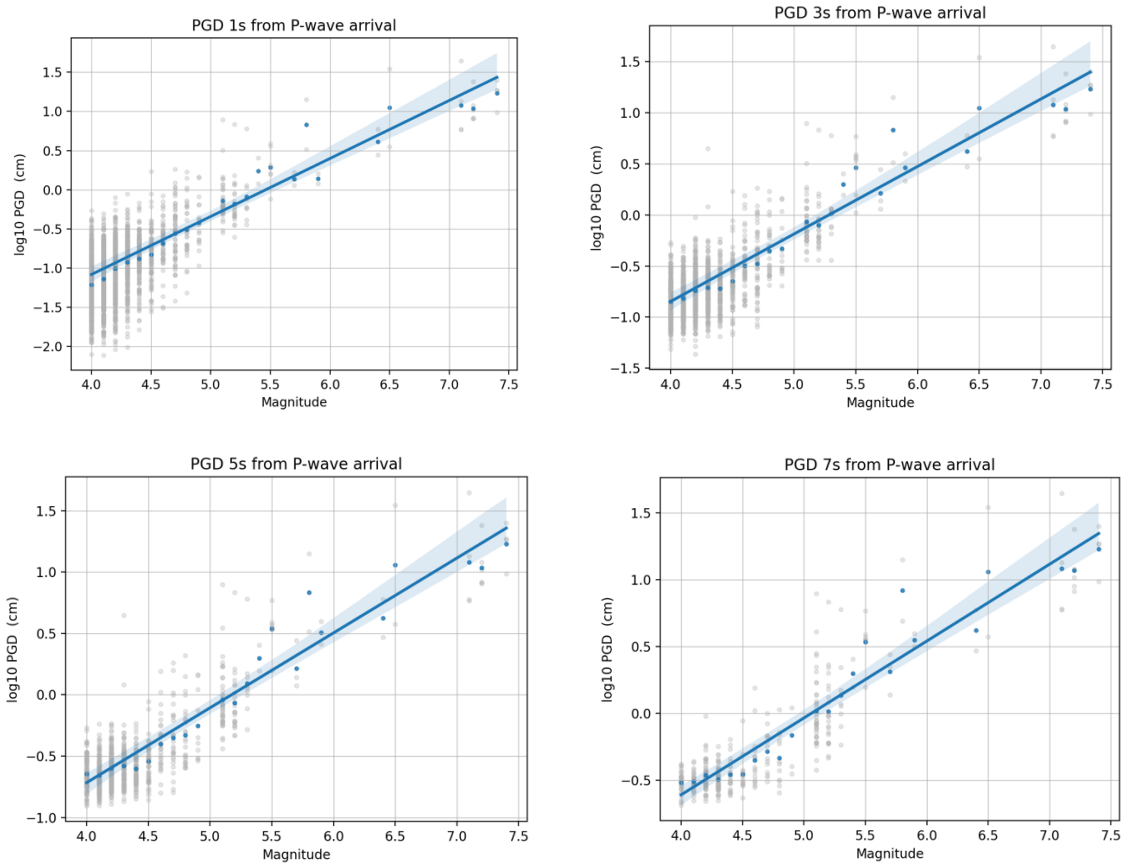

Figure 14. *Peak ground displacement caused by the p-wave. PGD increases with time and magnitude. It is, therefore, possible to proportionally relate magnitude and peak ground displacement. It directly depends on the time window of the measurement. To enquire the effect of using certain time windows and the quality of the prediction algorithm, we plotted the PGD of each event, the average of the PGD for each decimal magnitude, the regression line and its confidence interval.*

Earthquakes of stronger magnitude also fit the prediction very well, especially the 07-09-2021 Guerrero event. The PGD keeps increasing even for earthquakes with magnitudes larger than 6 with no obvious sign of saturation. With larger time windows, the PGD of every magnitude increases and the most significant growths are in the 5 to 5.5 magnitude category. However, given that the data set for magnitudes >6 is very sparse, this result is not conclusive.

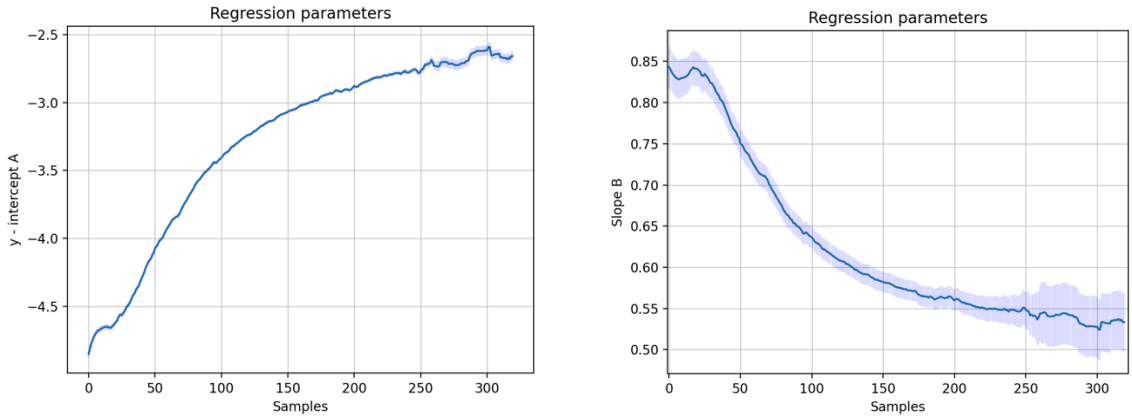

Figure 15. Evolution of the regression parameters, A and B, in the function of number of samples after the P-wave arrival. Y-intercept A on the left and slope B on the right, plotted with standard errors.

The plot of the y-intercept, the A parameter, of the regression shows how the lowest PGD gradually increased with the larger time windows, with the minimum being around -4.75 at 0 samples and -2.7 at 300 samples (≈ 10 seconds).

The slope, the B parameter, instead is a decreasing curve showing the lowering of the slope of the regression line. This is caused by more significant growth of PGD in lower magnitudes than in the higher ones. At magnitudes 4 to 4.5, the PGD goes from -1.25 cm in 1 second time window to -0.5 cm in 7 seconds time window. Instead, in higher magnitudes, the PGD changes slightly in the order of a couple of cents of centimetres.

There's an anomaly in the first 30 samples of the slope analysis, a local minimum, and then it grows for 15 samples and starts decreasing again. This anomaly is shown in the y-intercept graph as well; around the same sample, the curve stops growing for 15 samples.

After looking in detail at the data in this range of samples, it showed that there's a significant growth of PGD in the magnitudes 5 to 5.5, which is responsible for the increase of the regression slope and halt of the increase of the y-intercept.

The curves of the y-intercept and slope can be interpolated to describe the evolution of the parameter in time, having one function instead of 300 different parameters.

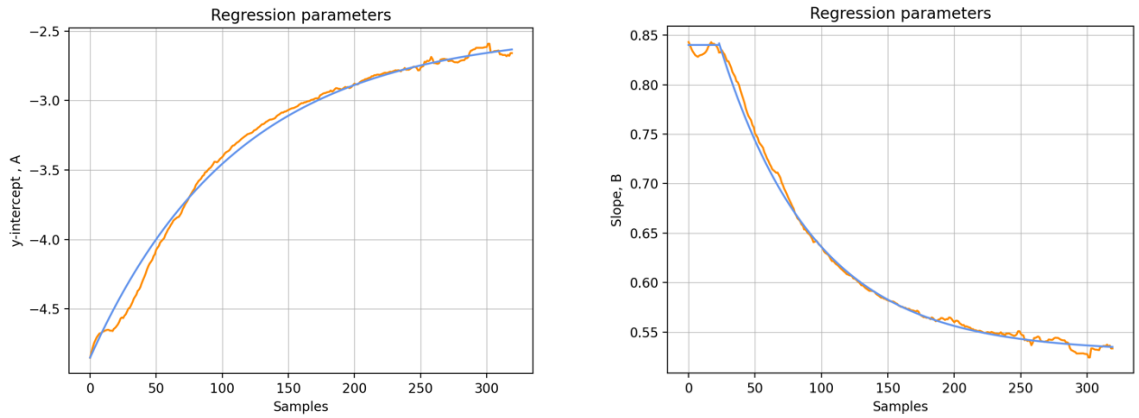

Figure 16. Curves of the evolution of the regression parameters fitted with two exponential functions.

We found that an exponential curve fits the curves best:

$$A, B = C\ (e^{D*samples}) + E$$

The coefficients in the function for the A and B parameters were:

Coefficients curve fit	y-intercept A	A - standard deviation errors	Slope B	B - standard deviation errors
C	-2.35	0.04	0.43	0.006
D	-0.009	0.0003	-0.014	0.0005
E	-2.5	0.02	0.53	0.02

The curve of the B parameter has a plateau in the first 23 samples of the plot. In order to keep the interpolation function simple while having a good fit with the curve, we opted to express the coefficients in two different functions, one exponential for the samples from 23 to 300, as shown before and one constant with y = 0.84 in the first 23 samples.

10. Discussion

The data used for this analysis, had multiple data gaps, as multiple stations through the analysed time span, had power and connectivity issues. Due to low or missing instrument maintenance in 2019, the data return dropped from ~70% in 2018 to 50% (Kuna et al., in prep.). This was conditioned by the fact that the network was in early stages of testing, the quality and reliability of the system has increased by the end of the time span used for the analysis. The expansion of the network to multiple countries will help highlight weak points of the system, also the improvement of the sensors design will significantly help solve connectivity problems and reduce maintenance needs. The results are inevitably conditioned by these technical outages of the stations, but still, we were able to extract some interesting conclusions.

As demonstrated in multiple studies, there's a saturation point in the time evolution of P wave peak ground displacements in the magnitude-displacement scaling, and it depends on the length of the P-wave time window (Trugman et al., 2019). In this study, we focused on the relation between the time length of P wave data and displacement and how it would correlate with magnitude. In the different time windows, there's a visible increase in displacement, especially for lower magnitudes, as the results of the regression parameters show quite well. No clear signs of saturation have been found, not even in the shortest time window of 1 second, where Trugman et al. (2019) measured saturation already in the 5.5 to 6 magnitude interval. Having just two earthquakes in the Mw 6-6.5 range and just 3 in the >7 makes it hard to extract any general conclusions about the functioning of the sensors. But even with sparse strong magnitude data, we can assess that the $\log_{10}$PGD scales very well with magnitude even for strong events, given the data we now have. This could be influenced by the fact that we were able to pick strong earthquakes also in stations farther away from the epicentre, which after the correction for the distance attenuation, would produce higher PGD.

To express the correlation of PGD and magnitude we did a regression analysis. The results of this analysis are the parameters A and B, expressing respectively the y-intercept and slope of the regression line. These parameters are the result that best describes the magnitude estimation algorithm, by defining the lowest PGD and the rate at which the PGD increases in relation to magnitude. The confidence interval shows a good level of certainty of the regression up to Mw 5.5, after the confidence interval is wider due to sparse and more variable data.

The explication of the evolution of the parameters, through an exponential function, significantly helps simplifying the magnitude equation, not having one parameter for each sample used, but instead having a function that describes the evolution of the parameter through the samples. This allows us to have one equation for all time windows, that accounts with the changes of the regression analysis and incorporates them into one equation.

11. Conclusion

Earthquakes can be catastrophic events and disrupt people's lives in a significant, and uncontrollable ways. EEW can help reduce earthquake's impact and provide people with a technology that would allow them to take action before the destructive waves strike *(Allen and Melgar. 2019)*.

This study aims to improve algorithms for magnitude calculation in Grillo/OpenEEW system. We demonstrated the correlation between the peak ground displacement and earthquake magnitude and their evolution with the increasing length of the P-wave segment. We defined this relationship through a regression analysis and produced an equation for magnitude calculation. It describes the evolution of the estimated magnitude through the different time windows, implementing in the equation also the time factor.

$$\log (PGD^{10km}) = A_t + B_t M_t$$

$$M = A_t - \frac{B_t}{\log (PGD^{10km})}$$

Where A and B are defined by the function:

$$A_t, B_t = C\ (e^{D*samples}) + E$$

Through this study, we can confirm the versatility of MEMS accelerometers, especially for EEW purposes, being low-cost and producing relatively accurate data. The “Grillo” network shows how impactful this technology can be, bringing costs down and improving performance.

It is a network still in development, so we have to take into account all the problems that are associated with it. Some stations weren’t located ideally, recording strong surrounding noise making it hard to handpick and document earthquakes. But this study shows the proof of the concept and what is actually achievable with such low-cost sensors. The Guerrero event is a clear demonstration of what this network is capable of, especially if the desired high density of stations is achieved. The biggest problem with earthquake analysis is the low amount of data. The diffusion of “Grillo” networks across multiple countries will noticeably help the research and development of this system, collecting significantly larger amounts of data.

The improvement of these systems will help us get the fate back into our hands, having time to take action before catastrophic events strike. Having still many flaws and problems, but with a great objective to strive towards.

References

Allen R. M. 2011. Earthquakes, early and strong motion warning. In Encyclopedia of Solid Earth Geophysics, ed. HK Gupta, pp. 226–33. Boston: Springer

Allen, Melgar. 2019. Earthquake Early Warning: Advances, Scientific Challenges, and Societal Needs. Review in Advance January 30, 2019, https://doi.org/10.1146/annurev-earth-053018-060457

Allen, R. M. and H. Kanamori (2003). The potential for earthquake early warning in southern California, Science 300, no. 5620, 786–789.

"CATÁLOGO DE SISMOS". Servicio Sismológic Nacional. *doi*:*10.21766/SSNMX/EC/MX*

Douglas, J 2003. "Earthquake ground motion estimation using strong-motion records: a review of equations for the estimation of peak ground acceleration and response spectral ordinates" (PDF). Earth-Science Reviews. 61 (1–2): 43–104.

Douglas, John. 2012. On the recovery of peak ground velocity and peak ground displacement from strong-motion records. In: 12th European Conference on Earthquake Engineering

Fu, J., Li, Z., Meng, H., Wang, J., & Shan, X. 2019. Performance Evaluation of Low-Cost Seismic Sensors for Dense Earthquake Early Warning: 2018–2019 Field Testing in Southwest China. Sensors (Basel, Switzerland), 19(9), 1999. https://doi.org/10.3390/s19091999

He, C., Huang, Q., Bai, X. et al. 2021. A Global Analysis of the Relationship Between Urbanization and Fatalities in Earthquake-Prone Areas. Int J Disaster Risk Sci 12, 805–820 (2021). https://doi.org/10.1007/s13753-021-00385-z

Hoshiba, M. & Ozaki, T. 2014. Earthquake Early Warning and Tsunami Warning of the Japan Meteorological Agency, and Their Performance in the 2011 off the Pacific Coast of Tohoku Earthquake https://doi.org/10.1007/978-3-642-12233-0-1.

Hongjie Li, Jianjing Zhang, and Yalei Tang. 2017. Testing Earthquake EarlyWarning Parameters, τmaxp , τc, and Pd, for Rapid Magnitude Estimation in the Sichuan, China, Region. Bulletin of the Seismological Society of America, Vol. 107, No. 3, pp. 1439–1450, June 2017, doi: 10.1785/0120160386

Heimann, S., M. Kriegerowski, M. Isken, S. Cesca, S. Daout, F. Grigoli, C. Juretzek, T. Megies, N. Nooshiri, A. Steinberg, et al. 2017. Pyrocko-An open-source seismology toolbox and library, doi: 10.5880/GFZ.2.1.2017.001.

平成 23 年度 気象庁関係予算決定概要. Japan Meteorological Agency. December 24, 2010. Retrieved April 1, 2012.

Kanamori, H. 2005. Real-time seismology and earthquake damage mitigation, Annual Review Earth Planet. Sci. 33, 195–214.

Krischer, Lion & Megies, Tobias & Barsch, Robert & Beyreuther, Moritz & Lecocq, Thomas & Caudron, Corentin & Wassermann, Joachim. 2015. ObsPy: A bridge for seismology into the scientific Python ecosystem. Computational Science & Discovery. 8. 014003. 10.1088/1749-4699/8/1/014003.

V. Kuna, D. Melgar, A. Meira. In prep. Evaluation of the Grillo sensor, a low-cost accelerometer for IoT-based Real-time seismology.

Lancieri, M., A. Fuenzalida, S. Ruiz, and R. Madariaga. 2011. Magnitude scaling of early-warning parameters for the Mw 7.8 Tocopilla, Chile, earthquake and its aftershocks, Bull. Seismol. Soc. Am. 101, no. 2, 447–463.

Melgar, D., A. Ruiz-Angulo, X. Pérez-Campos, B. W. Crowell, X. Xu, E. Cabral-Cano, M. R. Brudzinski, and L. Rodriguez-Abreu (n.d.). Energetic Rupture and Tsunamigenesis during the 2020 Mw 7.4 La Crucecita, Mexico Earthquake, Seismological Research Letters, doi: 10.1785/0220200272.

QGIS Development Team, 2021. QGIS Geographic Information System. Open Source Geospatial Foundation Project.

Shieh, J., Y. M.Wu, and R. M. Allen (2008). A comparison of τc and τmax p for magnitude estimation in earthquake early warning, Geophys. Res. Lett. 35, L20301,

doi: 10.1029/2008GL035611.

Tajima, F., Hayashida, T. “Earthquake early warning: what does “seconds before a strong hit” mean?”. Prog Earth Planet Sci 5, 63 (2018). doi: 10.1186/s40645-018-0221-6

Tellier, Lainé. Understanding MEMS-based digital seismic sensors. January 2017

Ting-Li Lin and Yih-Min Wu. (2010) Magnitude estimation using the covered areas of strong ground motion in earthquake early warning. GEOPHYSICAL RESEARCH LETTERS, VOL. 37, L09301, doi:10.1029/2010GL042797

Trugman, D. T., Page, M. T., Minson, S. E., & Cochran, E. S. (2019). Peak ground displacement saturates exactly when expected: Implications for earthquake early warning. Journal of Geophysical Research: Solid Earth, 124, 4642–4653. https://doi.org/10.1029/2018JB017093

Shieh, J., Y. M.Wu, and R. M. Allen (2008). A comparison of τc and τmax p for magnitude estimation in earthquake early warning, Geophys. Res. Lett. 35, L20301, doi: 10.1029/2008GL035611.

Villafuerte, C., V. M. Cruz-Atienza, J. Tago, D. Solano-Rojas, S. Franco, R. Garza-Girón, L. A. Dominguez, and V. Kostoglodov (2020). Slow slip events and megathrust coupling changes reveal the earthquake potential before the 2020 Mw 7.4 Huatulco, Mexico event, preprint, Earth and Space Science Open Archive.

Wolfe, C. (2006). On the properties of predominant-period estimators for earthquake early warning, Bull. Seismol. Soc. Am. 96, no. 5, 1961–1965.

Wu, Y. M., and Z. Li (2006). Magnitude estimation using the first three seconds P-wave amplitude in earthquake early warning, Geophys.Res. Lett. 33, L16312, doi:10.1029/2006GL026871.

Wu, Y. M., and H. Kanamori (2005b). Experiment on an onsite early warning method for Taiwan early warning system, Bull. Seismol. Soc. Am.95, 347–353.

Yamasaki,"What we can learn from Japan's early earthquake warning system," Momentum: Vol. 1: Iss. 1 , Article 2.

Zollo, A., M. Lancieri, and S. Nielsen (2006). Earthquake magnitude estimation from peak amplitudes of very early seismic signals on strong motion, Geophys. Res. Lett. 33, L23312.